J Mater Sci (2010) 45:2681–2687
DOI 10.1007/s10853-010-4249-2

Negative temperature coefficient thermistor based on $BaFe_xSn_{1-x}O_{3-\varepsilon}$ solid solutions

Changlai Yuan · Xinyu Liu · Yun Yang · Changrong Zhou

Received: 10 September 2009 / Accepted: 19 January 2010 / Published online: 6 February 2010

Abstract A negative temperature coefficient (NTC) thermistors based on $BaFe_xSn_{1-x}O_{3-\varepsilon}$ were fabricated by conventional solid-state reaction method. The microstructure and electrical properties of the NTC thermistors were characterized by X-ray diffraction (XRD), electric ($R(T)$), and impedance measurements. The XRD analysis shows that the $BaFe_xSn_{1-x}O_{3-\varepsilon}$ still remains cubic perovskite structure and the crystal growth orientation changes at higher Fe content. Similarly, the electric measurements indicates that all the samples show typical NTCR behavior; with increasing Fe content, the room temperature resistivity, activation energy, and thermistor constant decrease, are in the range of 2.52–217 KΩ cm, 0.343–0.43 eV, and 3900–4896 K, respectively. The impedance spectroscopy confirms that the observed ac resistance, consisting of the grain bulks, grain boundaries, and electrode–ceramic interface, mainly attributes to the grain boundaries and grain bulks; with the rise in temperature the grain boundary resistance shows more rapid change than the grain resistance; moreover, the Fe concentration can greatly affect the grain and grain boundary resistance.

C. Yuan (✉) · X. Liu · Y. Yang · C. Zhou
Guangxi Key Laboratory of Information Materials, Guilin University of Electronic Technology, 541004 Guilin, Guangxi, People's Republic of China
e-mail: yclguet@yahoo.com

C. Yuan · X. Liu
College of Materials Science and Engineering, Central South University, 410083 Changsha, People's Republic of China

Introduction

Negative temperature coefficient (NTC) resistors are found in an ever-increasing number of electrical and electronic products. The devices are largely based upon spinel or perovskite-like structure ceramic solid solutions. The major requirements for these systems are to display high thermistor constant, to have good stability (reproducibility) and the possibility of synthesising in ambient atmosphere [1]. Unfortunately the stability of spinel type materials is adequate only when the temperature is about 300 °C, for higher operating temperatures it is more appropriate to use perovskite materials which have a better thermal stability [2]. $BaSnO_3$ is a perovskite material of special importance due to its low permittivity, semiconducting behavior, and high thermal stability. The property of thermal stability up to 1200 °C makes it quite attractive as a ceramic material for many applications. The main drawback for this kind of materials is the requirement of high sintering temperatures (≥1500 °C) and high resistivity at room temperature. This factor necessitates suitable doping at the A/B sites for tailoring of its semiconducting properties and the sintered temperature lowering.

It has been reported that Pb^{2+} doping/substitution at the Ba-site of $BaSnO_3$ shows a typical negative temperature coefficient of resistance (NTCR) behavior like a semiconductor [3] and that Te^{4+} substitution at Sn-site caused a ferroelectric–paraelectric phase transition [4]. The effect of Ba or Sn site substitution in different stannates by transition metal (Co, Cr)/rare earth metal (La) and changes in the physical properties of the corresponding modified stannates has been reported [5–7]. Very little is known about electrical character of $BaSnO_3$ in which a partial substitution at the B sub-lattice (Sn sites) has been carried out. The NTC effect of the antimony substitution has been reported [8],

but no work (to our knowledge) has dealt with the Fe substitution. In the work, some structural and electric properties of iron-substituted stannum in $BaFe_xSn_{1-x}O_{3-\varepsilon}$-based ceramic compounds are highlighted and their sintered temperature can be lowered ($\leq$1350 °C). A variation of Fe concentration is expected to cause substantial changes in the electrical properties of the material because of relative difference in the cation size and valence.

Experimental procedures

A conventional ceramics fabrication technique was used to prepare the $BaFe_xSn_{1-x}O_{3-\varepsilon}$ ($0.5 \leq x \leq 0.9$) perovskite solid solutions. As to the compositions with $x \leq 0.5$, it is not worthy to investigate due to the high sintering temperature ($T > 1350$ °C) and resistivity. As the starting powders, we used analytical request (AR) grade $BaCO_3$, Fe_2O_3, and SnO_2 of appropriate proportions as shown in Table 1. The powders were mixed in acetone, dried, and then calcined at 1050–1150 °C for 6 h. The calcined powders with a binder (5 wt% polyvinyl alcohol) were uniaxially pressed into a disk with an 18 mm diameter and 1.5 mm thickness at 150 MPa. The disc samples directly placed on a platinum sheet were put in a furnace and heated at 1300–1350 °C (shown in Table 1) for 2 h in air. Using a fired on Ag paste, the electrodes were formed on polished ceramic surfaces for the electrical measurements.

The crystalline structure of the prepared samples was analyzed by an X-ray diffractometer (BRUKERD8-ADVANCE) using Cu Kα radiation with 40 kV, 35 mA, at a scanning rate of 6°/min. The microstructure of the samples was investigated by using a scanning electron microscope (Model: JSM5610LV). The samples of each composition were held with a holder in a tube furnace, and their temperatures were measured with a digital thermometer. The electrical resistance of the samples in the furnace was measured with a digital multimeter (Fluke 45) from 25 to 200 °C in steps of 5 °C. The accuracy of the furnace measurements is ±0.5 °C. The impedance measurements were performed in the frequency range from 40 Hz to 110 MHz at different temperatures, using an Agilent Impedance Analyzer (4294A) controlled by a personal computer. The impedance data were plotted in the complex plane, a plot of real component versus imaginary component. The samples were placed in a sample holder with a two-electrode configuration.

Results and discussion

The XRD patterns of the sintered compositions (Fig. 1) show the presence of single-phase cubic structure. All the peaks of the $BaFe_xSn_{1-x}O_{3-\varepsilon}$ samples were indexed on the basis of the published data of the host $BaSnO_3$, which indicates that the cubic crystal structure was retained even after the addition of Fe_2O_3 for all the compositions. The space group is consistent with the $BaSnO_3$ cubic structure (F_{m-3m}). But for composition $x = 0.9$, the peak intensity of (200) face instead of (110) face increases, the result shows the crystal growth orientation of the composition is along the (200) face rather than along the (110) face like the other compositions. The unit cell parameter a, exhibits a quasi-linear dependence against substitution level x, and decreases from 4.0958 to 4.0322 Å with the increase in iron content (The inset of Fig. 1). This is due to the fact that the

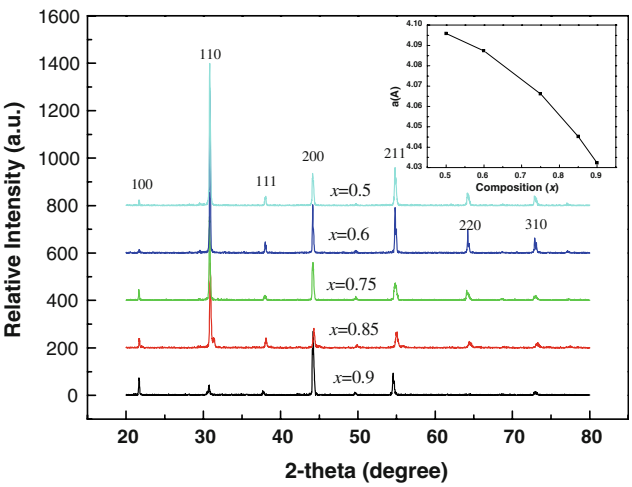

Fig. 1 XRD patterns of $BaFe_xSn_{1-x}O_{3-\varepsilon}$ sintered at 1300 °C to 1350 °C for 2 h (the *inset* represents the lattice parameter, a, evolution versus compositions (x) in the system of $BaFe_xSn_{1-x}O_{3-\varepsilon}$ solid solutions)

Table 1 The calculated $3 - \varepsilon$ value, oxygen vacancy, ρ_{25}, $B_{25/85}$ constant, and activation energy for different compositions (x) sintered at 1300–1350 °C for 2 h

Composition (x)	$x = 0.5$	$x = 0.6$	$x = 0.75$	$x = 0.85$	$x = 0.9$
Sintering temperature (°C)	1350	1335	1320	1310	1300
$(3 - \varepsilon)$ value	2.912	2.914	2.927	2.978	2.922
Oxygen vacancy	0.088	0.086	0.073	0.022	0.078
Room resistivity (KΩ cm)	217	22.5	6.15	4.05	2.52
$B_{25/85}$ constant (K)	4896	4686	4406	3900	3905
Activation energy(eV)	0.430	0.412	0.387	0.343	0.343

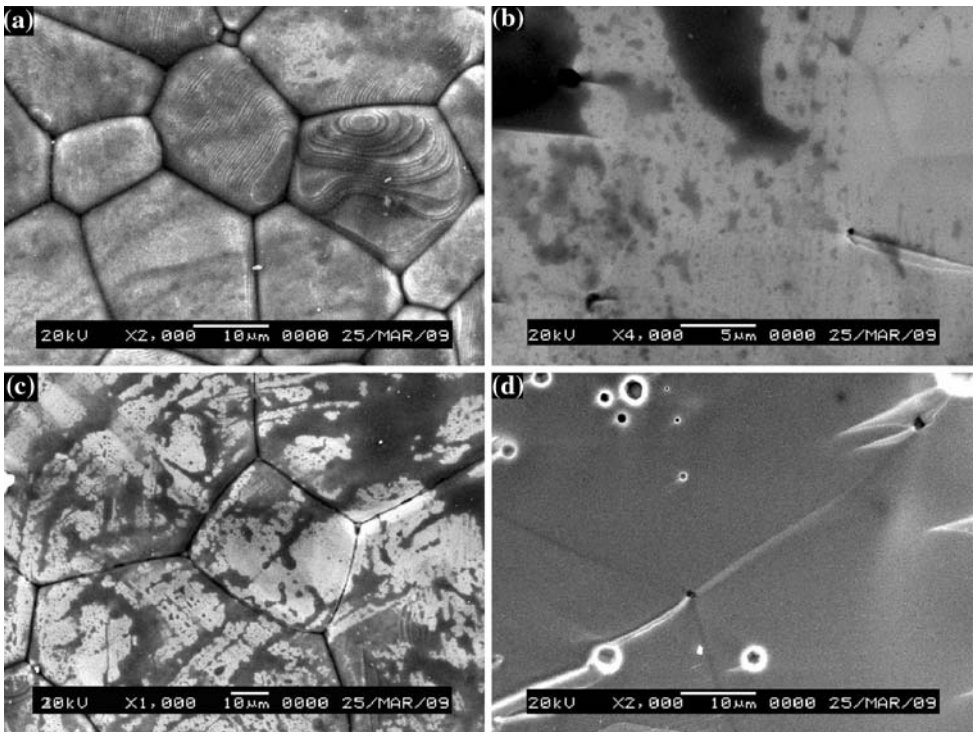

Fig. 2 SEM micrographs of $BaFe_xSn_{1-x}O_{3-\varepsilon}$ sintered samples: **a** the profile of composition $x = 0.75$, **b** the section of composition $x = 0.75$, **c** the profile of composition $x = 0.85$, and **d** the section of composition $x = 0.85$

Fe^{4+} or Fe^{3+} with smaller ionic radius ($r \leq 0.64$) merging into Sn-site ($r_{Sn^{4+}} = 0.71$) would decrease the cell parameters, which is similar to iron ionic of $BaCe_xFe_{1-x}O_{3-\varepsilon}$ [9].

The grain size of the as-sintered $BaFe_xSn_{1-x}O_{3-\varepsilon}$ ($0.5 \leq x \leq 0.9$) samples was found to have increased with increasing Fe content. For example, the SEM images from the surfaces and sections of the as-sintered $BaFe_{0.75}Sn_{0.25}O_{3-\varepsilon}$ and $BaFe_{0.85}Sn_{0.15}O_{3-\varepsilon}$ samples are shown in Fig. 2a–d, respectively. The grain boundaries among grains are very clear, the average grain sizes of the as-sintered $BaFe_{0.75}Sn_{0.25}O_{3-\varepsilon}$ and $BaFe_{0.85}Sn_{0.15}O_{3-\varepsilon}$ samples are about 20 and 50 μm, respectively. The grains keep close contact with each other from the section photos (Fig. 2b, d). It is apparent that the substituted Fe urges the grain growth during sintering and decreases the sintering temperature, because $BaFeO_{3-\varepsilon}$ is apt to form liquid phase at relative high temperatures, therefore, can increase the grain size of solid solution with the rise in Fe content.

The EDAX analysis (such as $x = 0.75$ as shown in Fig. 3) shows that the material contained Ba, Fe, Sn, and O. The calculated $3 - \varepsilon$ value and oxygen vacancy are shown in Table 1. By EDAX the oxygen vacancy concentrations of $BaFe_xSn_{1-x}O_{3-\varepsilon}$ are estimated to be about 0.088, 0.086, 0.073, 0.022, and 0.078, respectively. The ionic conductivity is primarily dependent on the oxygen vacancy concentration and the migration energy of oxygen ion at a certain temperature [10], so the existence of oxygen vacancy can be useful for the ionic conductivity. Based on

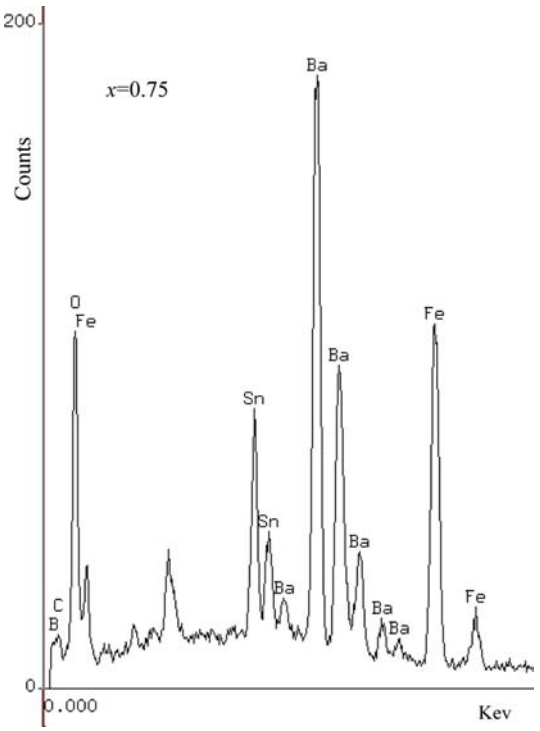

Fig. 3 EDAX spectra composition $x = 0.75$

the XRD and EDAX analysis, it is possible to postulate the following general formula for the solid solution:

$$Ba(Fe^{3+}_{2ex}Fe^{4+}_{x-2ex}Sn^{4+}_{1-x})O_{3-ex}, \quad (1)$$

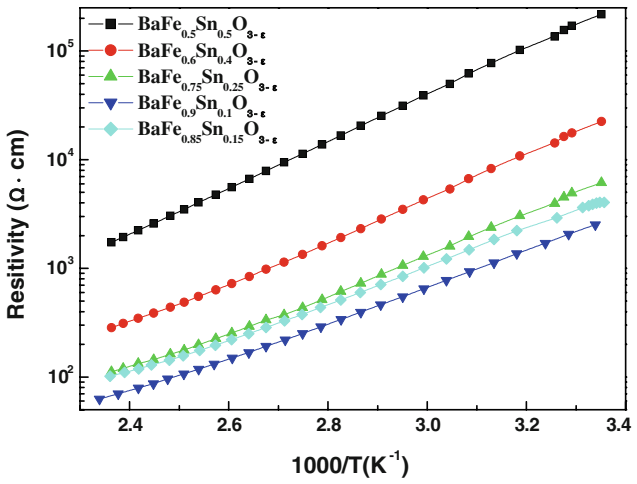

Fig. 4 Relation between the resistivities and reciprocal absolute temperatures ($1/T$) for the $BaFe_xSn_{1-x}O_{3-\varepsilon}$ thermistors

where *ex* stands for the oxygen vacancy, to maintain the equilibrium valence.

Figure 4 shows the electrical resistivity (ρ) of $BaFe_xSn_{1-x}O_{3-\varepsilon}$ ($0.5 \leq x \leq 0.9$) NTC thermistors with the temperature. The resistivity is exponentially lowered with increasing temperature. This feature is compatible with a process of charge transfer by hopping between localized states near to the top of the valence band or to the bottoms of the conduction band [11]. The room temperature resistivities, $B_{25/85}$ constant, and activation energy are also summarized in Table 1. The $B_{25/85}$ constant can be calculated by the following equation [12]: $B_{25/85} = (\ln\rho_1 - \ln\rho_2)/(1/T_1 - 1/T_2)$, where ρ_1 and ρ_2 are the resistivities measured at temperatures T_1 (25 °C) and T_2 (85 °C), respectively. According to Table 1, the values of $B_{25/85}$ constant and activation energy of the thermistors are in the range of 3900–4896 K and 0.343–0.430 eV, respectively. In particular, the ρ_{25} gradually decreased from 217 to 2.52 KΩ cm where the $B_{25/85}$ constant is still above 3900 K with the rise in compositions (x). It has already been reported [13] that at $YNi_xMn_{1-x}O_3$ system the predominant charge carriers are electrons when the percentage of Mn^{4+} is higher than that of Mn^{3+}. According to the formula 1 and Table 1, all the samples must have a percentage of Fe^{4+} higher than that of Fe^{3+}, therefore, the predominant charge carriers are electrons in bulk ceramic. Furthermore, based on the above results of unit cell parameter a, further addition of the doped iron will decrease the average metal–oxygen bond energy [14], the factor will make the transport of oxygen ions in the lattice become easier. As a result, continuing additions of Fe_2O_3 has a positive influence on the conductivity of $BaFe_xSn_{1-x}O_{3-\varepsilon}$ thermistor ceramics.

The above interpretation about conductive mechanism mainly involves into the ceramic body, but the interior region-like grain boundary (R_{gb}) and grain bulk (R_g) should not be neglected. Impedance spectroscopy has been used for probing the NTCR behavior in semiconducting ceramics because it is possible to separate the contribution of each *RC* (parallel resistance–capacitance) electrical component in the polycrystalline NTCR ceramics. This behavior of the electrical response obeys Cole–Cole's formalism [15].

The typical impedance spectra (Nyquist plot) of $BaFe_xSn_{1-x}O_{3-\varepsilon}$ samples at room temperature are shown in Fig. 5. It is known that the overall ac resistance of the samples can be determined from the intercepts in Im(Z) versus Re(Z) plots at low frequency. From the plots (Fig. 5a, b), it is seen that with increasing compositions x the ac resistance of the samples decreases. For compositions with $x = 0.5$, 0.6, and 0.75, the Im(Z) versus Re(Z) curve is composed of a overlapping semicircle (Fig. 5a), similar skewed semicircular arches are resolvable into three semicircles [16].When compositions with $x = 0.85$ and 0.9 the spectra (Fig. 5b) are one semicircle and one skewed semicircular arches which can be resolvable into two semicircles (the two contribution exhibiting overlapping). The semicircle at high frequencies indicates the effect of the grain bulk where the quasi-ideal behavior of the grain relaxation is seen, the relatively small one at low frequencies reflects the grain boundary contribution and the smallest one may represent the surface electrode effect (R_{el}) at lower frequencies [17]. In order to analyze the contribution degree of three components the experimental results are fitted using the nonideal equivalent circuit model as shown in the inset of Fig. 5a. In the circuit model each depressed semicircle is represented by parallel resistance-constant phase element (RCPE) circuit. The constant phase element (CPE) is expressed by Eq. 2 and defined by two values, C_0 and n,

$$C = C_0(j\omega)^{n-1} \tag{2}$$

where C_0 is expressed in units of capacitance component and ω is the angular frequency. The CPE tends to an ideal capacitance component when the exponent n tends to value 1, to a resistance component when $n = 0$, and to a Warburg component when $n = 0.5$. When CPE is placed parallel to a resistance, a Cole element is produced. In reality, few systems behave in a perfect Debye manner as represented by ideal resistors and capacitors, so in circuit model the nonideal capacitance CPE usually substitute for the ideal C. For the convenience of comparison the simulating impedance spectroscopy data of different Fe content are also plotted in Fig. 5a and b, and the plots indicate that the simulating line keeps good agreement with experimental line based on the simulating result of three parallel RCPE elements, which shows there are actually three parallel *RC* elements in the material, similar phenomenon is also found

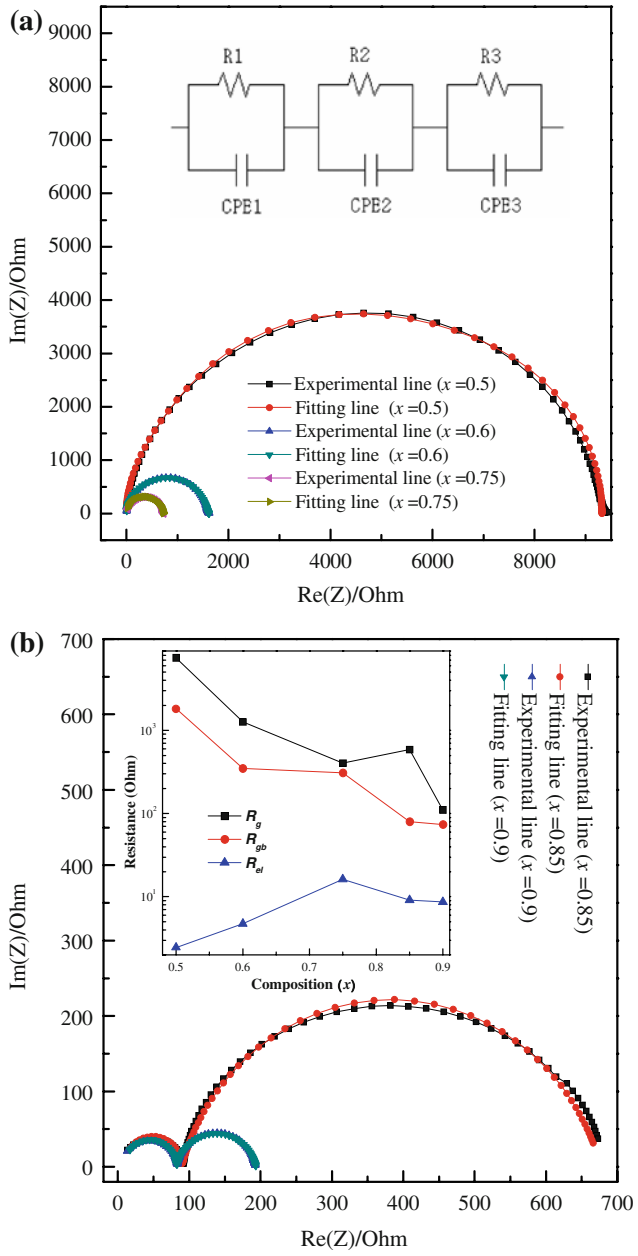

Fig. 5 Complex impedance spectrum of $BaFe_xSn_{1-x}O_{3-\varepsilon}$ at room temperature: **a** $x = 0.5$, 0.6, and 0.75 (the *inset* shows the equivalent circuit model); **b** $x = 0.85$ and 0.9 (*inset* of **b** shows the value of resistance R_g, R_{gb}, and R_{el}, as a function of compositions, x)

in $BaTiO_3$-based PTCR [18]. From the inset of Fig. 5b it can be seen that both R_g and R_{gb} decrease with increasing Fe substitution, but the resistance value of the additional electrical component at low frequency is almost constant and much small with the changed Fe content, which suggests the smallest additional component is accurately ascribed to the non-ohm touched resistance between the Ag electrode and the surface of ceramic body, and this resistance is indicative of a blocking contact (Schottky barrier) at the electrode–ceramic interface [18].

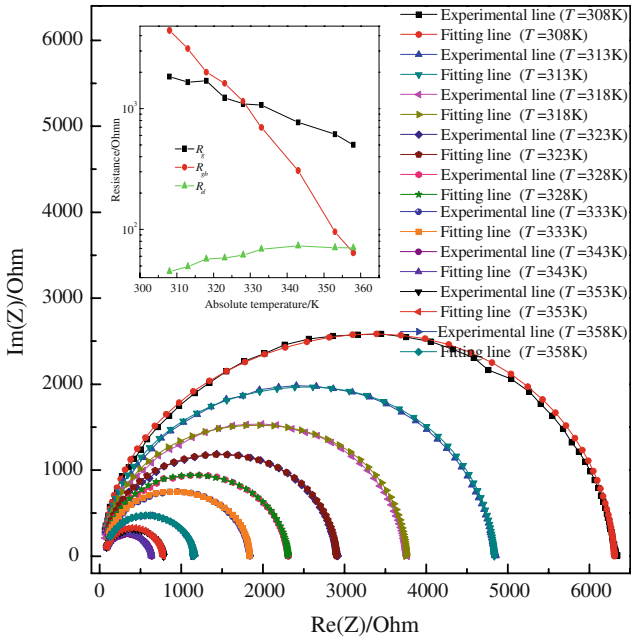

Fig. 6 Nyquist plots for $BaFe_{0.5}Sn_{0.5}O_{3-\varepsilon}$ taken at different temperatures for the composition $x = 0.5$ (the *inset* represents the value of resistance R_g, R_{gb}, and R_{el}, as a function of absolute temperatures)

Figure 6 shows the Nyquist plots (experimental and simulating impedance spectra) of $BaFe_{0.5}Sn_{0.5}O_{3-\varepsilon}$ over a wide frequency range (40 Hz–15 MHz) at nine temperatures (308–358 K) in the complex representation. The ac resistance (the resistance values intercepted in Im(Z) vs. Re(Z) plots at low frequency) of the sample was lowered with increasing temperature. The center of each semicircle is found to be depressed below the real axis, and this suggests that associated relaxation of ions is non-Debye in nature and confirms Jonscher universal frequency law [19]. At the same time, based on the simulating plots we can see that all the simulating results keep good agreement with the experimental plots, which indicates the nonideal equivalent circuit model (the inset of Fig. 5a) is consistent with fitting the thermistor system. According to the inset of Fig. 6, the R_{gb} and R_g show good NTC effect but the electrode effect is basically unchangeable with the rise in temperatures, and the thermistor constant of grain boundary is far larger than the grain.

Frequency dependence of Im(Z) are plotted as a function of composition x in Fig. 7a. In these plots, a peak appears corresponding to a particular polarization/relaxation process where the relation $RC = 1/\omega = 1/(2\pi f)$ is satisfied, where, R and C are the resistance and capacitance contribution of the RC circuit element corresponding to that process. The Im(Z) values in compositions with $x \leq 0.75$ show a Debye-like peak, indicating the presence of space charges. The peak frequency shifts to higher frequencies at higher Fe content,

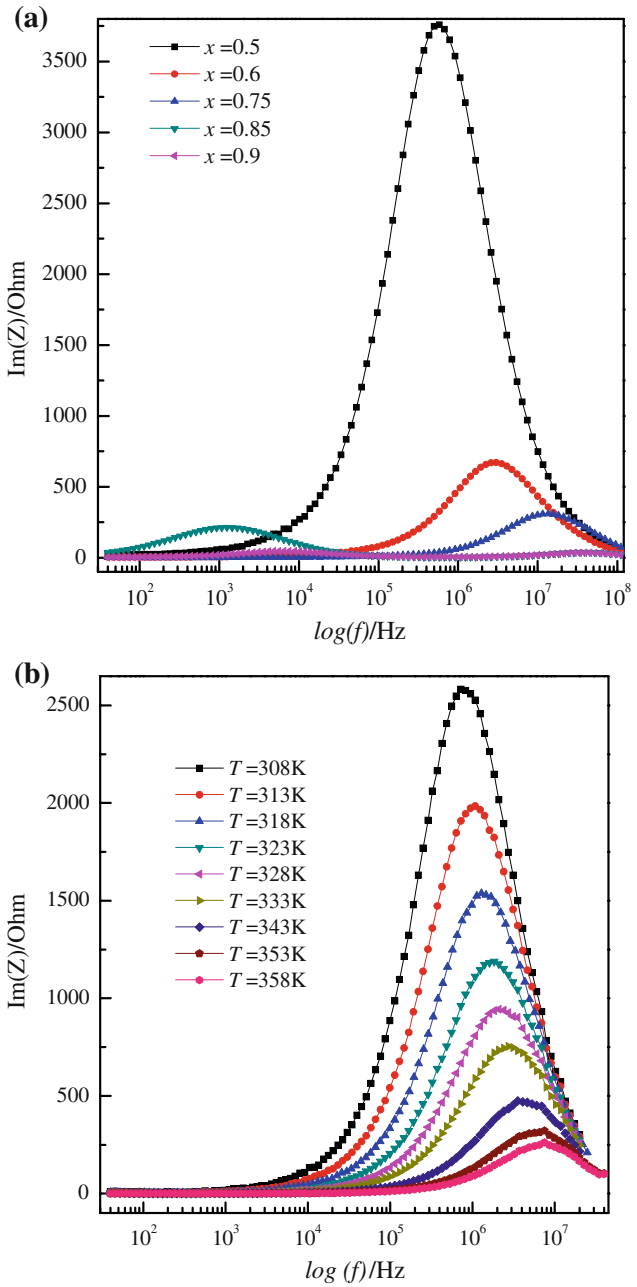

Fig. 7 Variation of imaginary part of impedance with frequency: **a** at various compositions and **b** as a function of frequency logarithmic at various temperatures

presenting the frequency and Fe concentration dependence of space charge characteristics. The peak amplitude of Im(Z) is proportional to the corresponding resistance [20]. For the compositions with $x = 0.85$ and 0.9, two peaks are observed, one in the low frequency range and another one in the high frequency range. The height of low frequency peak is higher than that of high frequency peak. This may be due to the release of space charges as a result of reduction in the barrier properties of materials with the rise in Fe concentration and may be responsible factor for the enhancement of ac-conductivity at higher frequencies. Similarly, the frequency of two peaks also shifts to higher frequencies at composition $x = 0.9$.

Figure 7b shows the variation of the imaginary part of the impedance with frequency (called loss spectrum) at different temperatures (308–358 K). The loss spectrum is characterized by two important features: (i) the appearance of only one peak in the loss spectrum $\mathrm{Im}(Z)_{\max}$; (ii) value of $\mathrm{Im}(Z)_{\max}$ decreases and shifts to higher frequencies with increasing temperature. Characteristic ii suggests that the spectral intensity of relaxation times is activated thermally in terms of hopping of charge carriers [21]. Apart from this, a shift in peak position in forward direction indicates that the relaxation time decreases with temperature. The two features show the relaxation species in the material may possibly be immobile species/electrons at low temperatures and defects/vacancies at high temperatures [22].

Conclusions

$BaFe_xSn_{1-x}O_{3-\varepsilon}$ ($x = 0.5 - 0.9$) samples have been prepared by solid-state reaction technique at 1300–1350 °C, and show good microstructure, homogeneity, and high sensitivity with wide operating temperature range. The R–T measurement of $BaFe_xSn_{1-x}O_{3-\varepsilon}$ samples indicates the values of ρ_{25}, activation energy E_a and $B_{25/85}$ constant tend to decrease with increasing Fe content, and are in the range of 2.52–217 KΩ cm, 0.343–0.43 eV, and 3900–4896 K, respectively. Impedance spectrum analysis reveals that the increasing substitution of Fe in $BaSnO_3$ has resulted in a decrease in the grain and grain boundary resistance of the material; both the grain resistance and the grain boundary resistance show typical NTC effect with the rise in Fe content. For data fitting, it may be most reasonable to employ an equivalent circuit of three RCPE in series.

References

1. Vakiv M, Shpotyuk O, Mrooz O, Hadzaman I (2001) J Eur Ceram Soc 21:1783
2. Feltz A (2000) J Eur Ceram Soc 20:2367
3. Kumar A, Singh BP, Choudhary RNP, Thakur AK (2006) Mater Chem Phys 99:150
4. Kumar A, Singh BP, Choudhary RNP, Thakur AK (2005) Mater Lett 59:1880
5. Prakash O, Kumar D (2000) J Mater Sci Mater Electron 12:165
6. Prakash O, Kumar D, Shrivastava KK, Dwivedi RK (2001) J Mater Sci 36:5805. doi:10.1023/A:1012904021501
7. Hadjarab B, Bouguelia A, Benchettara A, Trari M (2008) J Alloys Compd 461:360
8. Lu W, Jiang S, Zhou D, Gong S (2000) Sens Actuators 80:35
9. Zhu X, Wang H, Yang W (2006) Solid State Ionics 177:2917

10. Smyth DM (1991) Ferroelectrics 116:117
11. Marinova V, Sainov V, Lin SH, Hsu KY (2002) J Appl Phys 41:1860
12. Macklen ED (1979) Thermistors. Electrochemical Publications Ltd, Ayr, Scotland, p 33
13. Gutierrez D, Peña O, Duran P, Moure C (2002) J Eur Ceram Soc 22:567
14. Kharton VV, Shaula AL, Snijkers FMM, Cooymans JFC, Luyten JJ, Marozau IP, Viskup AP, Marques FMB, Frade JR (2006) J Eur Ceram Soc 26:3695
15. Cole KS, Cole RH (1941) J Chem Phys 9:341
16. Sinclair DC, West AR (1989) J Appl Phys 66:3850
17. Abram EJ, Sinclair DC, West AR (2001) J Electroceram 7:179
18. Heinen B, Waser R (1998) J Mater Sci 33:4603. doi:10.1023/A:1004433224704
19. Gerhardt R (1994) J Phys Chem Solids 55:1491
20. Liu J, Duan CG, Mei WN, Smith RW, Hardy JR (2005) J Appl Phys 98:093703
21. Prasad NV, Narendra Babu S, Siddeshwar A, Prasad G, Kumar GS (2009) Ceram Int 35:1057
22. Barik SK, Choudhary RNP, Mahapatra PK (2008) J Mater Sci Mater Electron 19:607